

The chemical sensitivity of X-ray spectroscopy: high energy resolution XANES versus X-ray emission spectroscopy of substituted ferrocenes†

Cite this: *Phys. Chem. Chem. Phys.*, 2013, **15**, 8095

Andrew J. Atkins,^a Matthias Bauer^{*b} and Christoph R. Jacob^{*a}

X-ray spectroscopy at the metal K-edge is an important tool for understanding catalytic processes and provides insight into the geometric and electronic structures of transition metal complexes. In particular, X-ray emission-based methods such as high-energy resolution fluorescence detection (HERFD), X-ray absorption near-edge spectroscopy (XANES) and valence-to-core X-ray emission spectroscopy (V2C-XES) hold the promise of providing increased chemical sensitivity compared to conventional X-ray absorption spectroscopy. Here, we explore the ability of HERFD-XANES and V2C-XES spectroscopy to distinguish substitutions beyond the directly coordinated atoms for the example of ferrocene and selected ferrocene derivatives. The experimental spectra are assigned and interpreted through the use of density functional theory (DFT) calculations. We find that while the pre-edge peaks in the HERFD-XANES spectra are affected by substituents at the cyclopentadienyl ring containing π -bonds [A. J. Atkins, Ch. R. Jacob and M. Bauer, *Chem.–Eur. J.*, 2012, **18**, 7021], the V2C-XES spectra are virtually unchanged. The pre-edge in HERFD-XANES probes the weak transition to unoccupied metal d-orbitals, while the V2C-XES spectra are determined by dipole-allowed transitions from occupied ligand orbitals to the 1s core hole. The latter turn out to be less sensitive to changes beyond the first coordination shell.

Received 6th March 2013,
Accepted 22nd March 2013

DOI: 10.1039/c3cp50999k

www.rsc.org/pccp

1 Introduction

X-ray spectroscopy at synchrotrons, mainly X-ray absorption spectroscopy (XAS), is nowadays a powerful tool to study chemical processes,^{1–8} such as catalysis by transition metal complexes.^{9–13} To be specific to a catalytic center of interest, such studies are typically performed at the metal edge, *i.e.*, core electrons of a central metal atom are excited. However, the information content of XAS is mainly limited to type, number, and distances of coordinating atoms as well as qualitative oxidation states of the central metal atom (for examples, see ref. 14–18). The details of the electronic structure related to the d-electrons of transition metal complexes can usually not be resolved with conventional XAS. Moreover, the sensitivity to light atoms is generally limited to the nearest neighbor shell, while XAS is “blind” to changes beyond the directly

coordinating atoms.^{19,20} Changes in the electronic structure caused by structural modifications in this second coordination shell can hardly be detected. Since XAS investigations enable *in situ* studies under nearly any experimental condition without adopting the system parameters to the experiment,^{21,22} it would be highly desirable to overcome these limitations. This would greatly increase the applicability of X-ray spectroscopy for studying chemical processes in catalysis.

X-ray emission-based methods open new opportunities for chemical research at synchrotron sources in this direction. They are based on the high energy resolution detection of the fluorescence radiation emitted by a sample after irradiation with X-rays.²³ To achieve an appropriate resolution, a dedicated experimental setup consisting of a high flux, high brilliance synchrotron X-ray source and a Rowland-type spectrometer equipped with analyzer crystals as shown in Fig. 1 is usually employed.²³ The usage of analyzer crystals in combination with a double crystal monochromator (DCM) either allows for the recording of X-ray absorption near edge structure (XANES) spectra by monitoring the intensity of a selected fluorescence decay channel while sweeping the incident energy of the DCM or the measurement of X-ray emission spectra (XES) by keeping the incident energy constant, at a value above the

^a Karlsruhe Institute of Technology (KIT), Center for Functional Nanostructures and Institute of Physical Chemistry, Wolfgang-Gaede-Str. 1a, 76131 Karlsruhe, Germany. E-mail: christoph.jacob@kit.edu

^b TU Kaiserslautern, Fachbereich Chemie, Erwin-Schrödinger-Str. 54, 67663 Kaiserslautern, Germany. E-mail: bauer@chemie.uni-kl.de

† Electronic supplementary information (ESI) available. See DOI: 10.1039/c3cp50999k

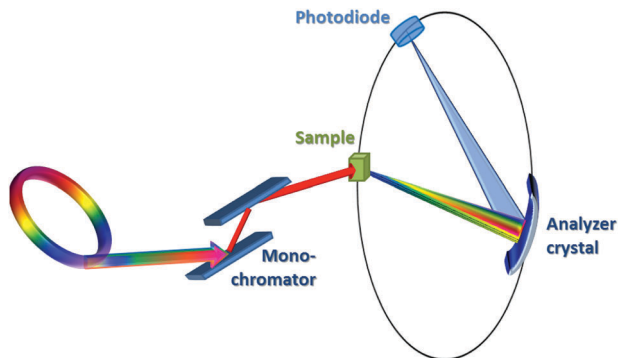


Fig. 1 Schematic representation of the experimental setup required for X-ray emission-based spectroscopic methods. This setup can be employed both for recording HERFD-XANES and V2C-XES spectra.

edge, and sweeping the analyzer crystals over a selected range of emission energies.

As long as non-local effects are absent, the described mode of recording XANES spectra is formally equivalent to conventional XANES experiments,²³ in which all fluorescence channels are summed up to yield the total absorption cross section $\sigma_{\text{abs}} = \sum_i \sigma_i$. However, by selecting a single fluorescence channel, an energy resolution smaller than the life-time of the final state of the absorption process can be reached.^{24,25} This final state in the case of K-edge XANES spectra is characterized by a 1s core hole and an additional electron in an empty electronic state. Experiments using a setup as shown in Fig. 1 are called high energy resolution fluorescence detection XANES (HERFD-XANES).^{26,27} They can be used to probe unoccupied electronic states with a resolution not available in conventional XAS.

Alternatively, in a so-called valence-to-core (V2C) XES experiment, the 1s electron is non-resonantly excited into the continuum far above the ionization threshold, and the following radiative relaxation of a valence electron into the core hole is detected. This valence electron originates from an occupied electronic state. While sweeping the emission energy, the different occupied states are thus probed in a $K\beta_{2,5}$ (V2C) emission experiment. The $K\beta_{2,5}$ emission process is reduced by a factor of 500 and around 60 in intensity compared to the $K\alpha$ and $K\beta_{1,3}$ emission where the core hole is filled with low-lying 2p and 3p electrons, respectively, but it is the only transition with sufficient sensitivity to ligand effects.²⁸ As the occupied valence states are strongly determined by the chemical environment of the central metal atom, this method is also sensitive to the identity of the ligands as well as the geometry of the immediate ligand environment in catalytically active metal complexes.^{29,30} Fig. 2 summarizes the transitions of the two described methods.

Note that these two techniques provide complementary information:¹² By means of V2C-XES and HERFD-XANES, details about both occupied and unoccupied electronic states, respectively, are available under almost any experimental condition. For the interpretation of such X-ray spectra, and for relating the observed transitions to the electronic structure, quantum chemical calculations are essential (for reviews, see,

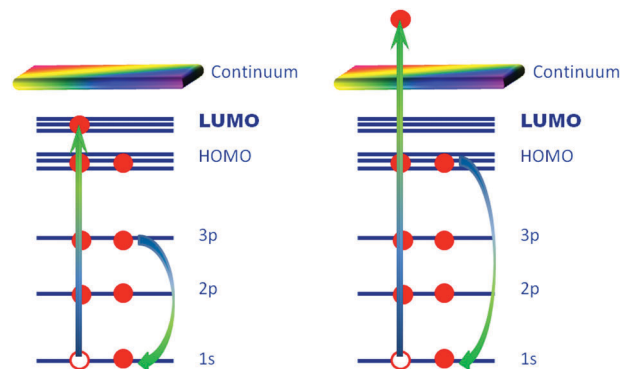


Fig. 2 Qualitative representation of the processes observed in HERFD-XANES (left) and V2C-XES (right) within a molecular orbital picture. In HERFD-XANES, a core electron is excited to unoccupied molecular orbitals and the intensity of the $K\beta_{1,3}$ emission is measured, whereas in V2C-XES, the relaxation of an electron from an occupied molecular orbital following the creation of a core hole is probed.

e.g., ref. 31 and 32). In many cases, already rather simple approaches based on (time-dependent) density functional theory (DFT)^{33–38} can guide the assignment and interpretation of X-ray spectra.^{39–41}

Recently, we have demonstrated that HERFD-XANES at the Fe K-edge is able to detect subtle differences in the electronic structure induced by structural changes beyond the directly coordinating atoms.²⁰ This was shown for substituted ferrocenes, where the cyclopentadienyl rings constitute the first coordination shell, whereas substituents at these cyclopentadienyl rings can be considered as a second coordination shell. Such ferrocene-derived compounds play an important role in catalysis,⁴² in particular in bimetallic catalytic systems.¹⁰ Consequently, ferrocene and its derivatives^{40,43–45} as well as other metallocenes^{43,46,47} have been studied extensively using X-ray spectroscopic methods. The ability to extend the sensitivity of hard X-ray spectroscopy beyond the direct coordination environment provides an important new tool for such studies. Here, we want to explore whether V2C-XES is able to distinguish ferrocenes bearing different substituents at the cyclopentadienyl rings as well. To this end, we utilize the same model complexes considered earlier for HERFD-XANES, and analyze the experimental spectra with the help of quantum chemical calculations.

This work is organized as follows. Section 2 outlines the methodology used for the experimental measurements and for the quantum-chemical calculations. In Section 3 we discuss the HERFD-XANES and V2C-XES spectra and explore the chemical sensitivity of V2C-XES. Finally our conclusions are presented in Section 4.

2 Methodology

2.1 Experimental

All compounds were purchased from commercial providers with high purity (>98%) and used as received. Sample handling in the case of air sensitive complexes was carried out under an

argon atmosphere in a glove box. The samples were diluted with BN in a ratio of approximately 1 : 4 to avoid self-absorption effects.

The HERFD-XANES and XES experiments were performed at beamline ID26 at the European Synchrotron Radiation Facility.⁴⁸ The electron energy was 6.0 GeV, and the ring current varied between 180 and 200 mA. The measurements were carried out using two u35 undulators. The incident energy was selected using the $\langle 311 \rangle$ reflection from a double Si crystal monochromator. The energy calibration was performed using an iron foil. The incident X-ray beam had a flux of approximately 2×10^{13} photons per second at the sample position. All spectra were measured using an X-ray emission spectrometer with a sample and a crystal analyzer in the horizontal plane with respect to the storage ring.^{24,49} However, the sample, the analyzer crystal, and the photon detector (avalanche photodiode) were arranged in a vertical Rowland geometry.²³

The HERFD-XANES spectra as well as the experimental procedure used to obtain them have been described previously.²⁰ Valence-to-core K β XES spectra were recorded off resonance at an excitation energy of 7300 eV. Emission was recorded in the range of 7020–7130 eV, with a step width of 0.3 eV over the K $\beta_{2,5}$ emission line (7080–7130 eV). The emission energy was selected using the $\langle 662 \rangle$ reflection of five spherically bent Ge crystal analyzers. The total fluorescence yield (TFY) was monitored by a photodiode installed at about 90° scattering angle and at 45° to the sample surface. The intensity of the fluorescence radiation was normalized to the incident flux measured using an ionization chamber. The spectrometer energy was calibrated using the elastic line.

Samples were positioned at 45° to the beam and maintained at 15 K using a closed-cycle Helium cryostat. A helium-filled bag was used to reduce absorption of the fluorescence radiation between the cryostat and the spectrometer. All samples were checked for radiation damages, and no radiation damages could be detected within the acquisition time for the different spectra. Moreover, measurements were carried out on multiple spots on the samples.

Normalization and alignment of the spectra relative to each other was carried out according to Glatzel and Bergmann²³ using the K β main line (see also ref. 50). After subtraction of the tail of the K β main line with a spline, the spectra were deconvoluted by adjustment of pseudo-Voigt lines in a least-square fit. In these fits, all parameters (*i.e.*, intensity, full width at half maximum, and energy) were allowed to vary.

2.2 Computation of X-ray spectra

All calculations have been performed using (time-dependent) DFT within the ADF program package.^{51–53} The molecular structures of the substituted ferrocene complexes have been optimized employing the BP86 exchange–correlation functional^{54,55} and the TZP basis set, and are identical to those used in our earlier work.²⁰ For all considered compounds, the ground-state is the low-spin state ($S = 0$).

The XANES spectra have been calculated using time-dependent density functional theory (TD-DFT). To selectively target core excitations, the TD-DFT calculations were restricted to excitations originating from the Fe 1s orbital (restricted-channel

approximation).^{56,57} Such restricted-channel TD-DFT calculations have been applied extensively for K-edge XAS spectra of transition metal complexes.^{34,38,58–61} The QZ4P Slater-type orbital basis set was applied in all TD-DFT calculations. To judge the sensitivity of our results to the exchange–correlation functional, we employed both the non-hybrid functional BP86 and the hybrid functional B3LYP.^{62,63}

In our XAS calculations, the BP86 spectra were shifted by 183.39 eV and the B3LYP spectra by 152.62 eV for comparison with experiment. These shifts are chosen such that the energy of the pre-edge peak in ferrocene agrees with experiment. While these shifts are rather large, they do not affect the relative position of the peaks significantly. For Fe K-edge XAS, it has been demonstrated previously that despite the large absolute errors, the TD-DFT approach used here can provide relative excitation energies and intensities with an accuracy that allows for a direct comparison with experiment.³³ The relative excitation energies are determined by the valence orbitals and, therefore, not affected significantly by errors in the description of the core orbital. The largest part of the shift in the absolute excitation energies is due to the neglect of relativistic effects for the 1s core orbital. Including scalar relativistic effects with the zeroth-order regular approximation (ZORA)^{64,65} reduces the shifts to 58.84 eV for BP86 and to 27.51 eV for B3LYP, but does not change the overall spectra (see Fig. 1 in the ESI†). The remaining absolute errors are caused by the neglect of core-hole relaxation, insufficiencies of the exchange–correlation functionals, the use of a finite basis set, and the neglect of environmental effects. Core-hole relaxation could be included within the static-exchange approximation (STEX),^{66–68} the transition potential method,^{69–71} Δ SCF(-DFT) approaches,^{72,73} or by combining TD-DFT with a complex polarization propagator.^{74,75} However, these methods are computationally more demanding than restricted-channel TD-DFT and less robust when applied to transition metal complexes. Moreover, so far they have mainly been applied in the soft X-ray regime and their reliability for X-ray spectroscopy at the Fe K-edge (*i.e.*, in the hard X-ray regime) will have to be assessed in future work (for a comparison of Δ SCF-DFT and TD-DFT at the Cu K-edge, see ref. 73, and for Δ SCF-DFT calculations at the Mn K-edge, see ref. 76).

Within the dipole approximation, the intensities of the XANES transitions from the initial state i to the final state f are proportional to the electric-dipole oscillator strengths,

$$f_{if}^{(\mu^2)} = \frac{2m_e}{3e^2\hbar^2} E_{if} \langle i | \hat{\mu} | f \rangle^2, \quad (1)$$

where m_e and e are the mass and charge of the electron, respectively, E_{if} is the transition energy between the initial and final states, and $\hat{\mu}$ is the electric dipole operator. However, for metal K-edge XAS, one has to go beyond the dipole approximation and include higher order contributions.^{33,34} Most important are the electric-quadrupole oscillator strength,

$$f_{if}^{(Q^2)} = \frac{m_e}{20e^2\hbar^4 c^2} E_{if}^3 \left[\sum_{\alpha\beta} \langle i | \hat{Q}_{\alpha\beta} | f \rangle^2 - \frac{1}{3} \left(\sum_{\alpha} \langle i | \hat{Q}_{\alpha\alpha} | f \rangle \right)^2 \right], \quad (2)$$

where c is the speed of light, and $\hat{Q}_{\alpha\beta}$ is the electric-quadrupole operator with α and β being x , y or z , and the magnetic-dipole oscillator strengths,

$$f_{if}^{(m^2)} = \frac{2m_e}{3e^2\hbar^2} E_{if}^3 (\text{Im}\langle i|\hat{m}|f\rangle)^2, \quad (3)$$

where \hat{m} is the magnetic-dipole operator. However, as was pointed out by Neese and co-workers,³⁴ including these two additional contributions renders the intensities origin-dependent. This can be addressed by consistently including all contributions that are of the same order in the wave vector,⁷⁷ which leads to two additional interference terms, an electric-dipole–electric-octupole contribution,

$$f_{if}^{(\mu O)} = -\frac{m_e}{45e^2\hbar^4 c^2} E_{if}^3 \sum_{\alpha\beta} \langle i|\hat{\mu}_\beta|f\rangle \langle i|\hat{O}_{\alpha\beta}|f\rangle, \quad (4)$$

where $\hat{O}_{\alpha\beta}$ is the electric-octupole operator, and an electric-dipole–magnetic-quadrupole contribution,

$$f_{if}^{(\mu M)} = -\frac{m_e}{3e^2\hbar^3 c} E_{if}^2 \sum_{\alpha\beta\gamma} \varepsilon_{\alpha\beta\gamma} \langle i|\hat{\mu}_\beta|f\rangle \text{Im}\langle i|\hat{M}_{\gamma\alpha}|f\rangle, \quad (5)$$

where $\hat{M}_{\gamma\alpha}$ is the magnetic-quadrupole operator. In the present work, all XAS and XES intensities have been calculated using the full, origin-independent expressions [eqn (1)–(5)]. For the XAS spectra, these results are consistent with our previous work²⁰, in which we did not include these additional interference terms but instead placed the origin at the absorbing iron atom. With this choice of the origin, the additional interference terms, $f_{if}^{(\mu O)}$ and $f_{if}^{(\mu M)}$, become negligible.

For the calculation of XES spectra, we follow the work of Lee *et al.*³⁶ (see also ref. 78–80 and references therein for earlier work). This is a frozen orbital, one-electron Δ DFT approach which uses orbital energy differences between occupied orbitals, $\varepsilon_{1s} - \varepsilon_i$, to model the X-ray emission energies. Even though it is the simplest possible approximation for the calculation of XES spectra, it has been shown to work reliably for V2C-XES spectra of transition metal complexes.^{29,30,36,38,40,80} We employed the QZ4P basis set and used both the nonhybrid exchange–correlation functional BP86 and the hybrid functional B3LYP.

The calculated V2C-XES spectra were shifted by 182.86 eV and 148.82 eV for BP86 and B3LYP, respectively, where these shifts are chosen such that the energy of the highest energy V2C-XES peak in ferrocene agrees with experiment. As discussed above for the XAS spectra, the largest contributions to these shifts originate from the neglect of relativistic effects, the neglect of core–hole relaxation, and the errors in the exchange–correlation functional. If scalar-relativistic corrections are included *via* the ZORA approximation, the shifts are reduced to 58.36 eV for BP86 and 23.79 eV for B3LYP, but the overall V2C-XES spectra do not change (see Fig. 2 and Table SI in the ESI†). These shifts could be further reduced by accounting for core–hole relaxation, for instance by applying Δ SCF-DFT or transition potential DFT to XES spectroscopy (for reviews, see ref. 31 and 79). However, it has been demonstrated that for metal K-edge V2C-XES of transition metal complexes, the

absolute errors corrected by these shifts do not affect the relative excitation energies and the calculated intensity patterns significantly.^{29,36} For calculating XES intensities, we employed the origin-independent approach described above, where the initial and final states in the transition moments are now calculated between the Fe 1s core orbital and other occupied orbitals.

The calculated XAS spectra are plotted using Gaussian peaks with a full-width at half maximum (FWHM) of 0.7 eV, whereas for the XES spectra a FWHM of 1.5 eV is used.

3 Results

To compare the chemical sensitivity of HERFD-XANES and V2C-XES, in particular their ability to detect changes in the electronic structure induced by substitutions in the second coordination shell, we consider ferrocene and complexes derived from it. Our test set, shown in Fig. 3, consists of ferrocene (FeCp_2) and ferrocene derivatives containing substituents on the cyclopentadienyl (Cp^-) rings. In acetylferrocene ($\text{Fe}(\text{Cp})(\text{CpAc})$) and in vinylferrocene ($\text{Fe}(\text{Cp})(\text{CpVinyl})$) this substituent contains a π -bond that is conjugated with the cyclopentadienyl ring, whereas in 1,1'-bis-diphenylphosphinoferrrocene ($\text{Fe}(\text{CpPPH}_2)_2$) and in 1,1'-bis-diisopropylphosphinoferrrocene ($\text{Fe}(\text{CpP}^i\text{Pr}_2)_2$) there are phosphine substituents at both cyclopentadienyl rings. In addition, ferrocenium ($[\text{FeCp}_2]^+$) is included within the test set. Note that in all these six complexes, the first coordination shell around the iron atom is identical, whereas the different substituents are part of the second coordination sphere.

Fig. 4 shows the experimental HERFD-XANES spectra (left) and V2C-XES spectra (right) for this set of molecules. The HERFD-XANES spectra have been discussed earlier in ref. 20. Of particular interest are the pre-edge peaks, highlighted in

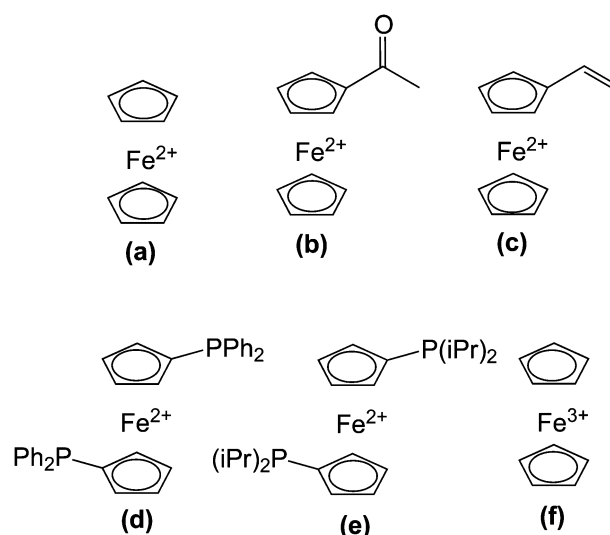


Fig. 3 Lewis structures for the test set of molecules considered in this work. (a) Ferrocene (FeCp_2), (b) acetylferrocene ($\text{Fe}(\text{Cp})(\text{CpAc})$), (c) vinylferrocene ($\text{Fe}(\text{Cp})(\text{CpVinyl})$), (d) 1,1'-bis-diphenylphosphinoferrrocene ($\text{Fe}(\text{CpPPH}_2)_2$), (e) 1,1'-bis-diisopropylphosphinoferrrocene ($\text{Fe}(\text{CpP}^i\text{Pr}_2)_2$), and (f) ferrocenium ($[\text{FeCp}_2]^+$).

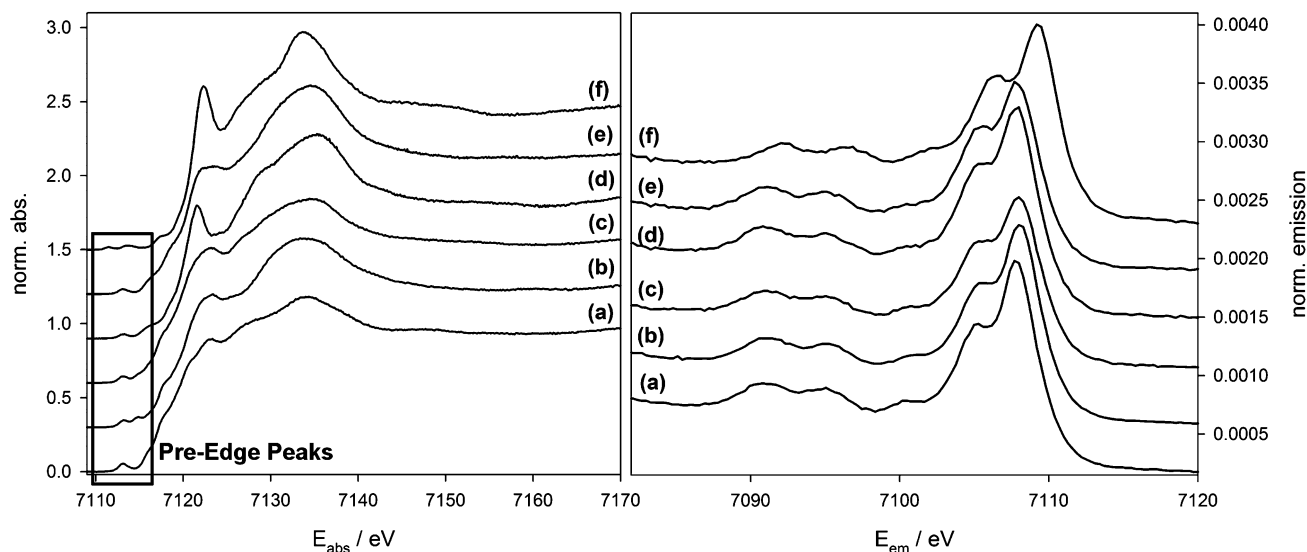


Fig. 4 Experimental HERFD-XANES spectra (left) and V2C-XES spectra recorded at an excitation energy of 7300 eV (right). The labels (a)–(f) refer to the ferrocene derivatives as listed in Fig. 3.

Fig. 4, which are due to transitions to the lowest unoccupied electronic states, since they are very sensitive to subtle changes in the electronic structure at the iron center. In acetyl- and vinylferrocene, the single pre-edge peak present in ferrocene is split into two separate peaks. In contrast, the V2C-XES spectra of ferrocene, acetylferrocene, and vinylferrocene are virtually identical. For the ferrocene derivatives bearing phosphine substituents, $\text{Fe}(\text{CpPPH}_2)_2$ and $\text{Fe}(\text{CpP}^i\text{Pr}_2)_2$, there are no differences in the single HERFD-XANES pre-edge peak, but obvious changes are found in the higher energy XANES region, in particular between 7117 and 7125 eV. On the other hand, the V2C-XES spectra appear identical to those of ferrocene. Finally, in ferrocenium the increased oxidation state of the iron center leads to significant changes in the pre-edge region and shifts the ionization edge to higher energies. Even in this case, the V2C-XES spectrum is shifted to higher energies, but remains qualitatively unchanged. For a detailed comparison of the V2C-XES spectra of ferrocene and ferrocenium, which differ in the oxidation state of the iron atom, we refer to ref. 40. In the following, we will focus on the $\text{Fe}(\text{II})$ complexes (a)–(e).

In our earlier work,²⁰ the differences in the pre-edge peaks in the HERFD-XANES spectra have been related to changes in the underlying electronic structure with the help of TD-DFT calculations. As a starting point for the further discussion of the V2C-XES spectra, we will briefly recall these results here. A qualitative molecular orbital (MO) diagram for ferrocene is shown in Fig. 5, in which the orbitals – shown as isosurface plots – as well as their ordering have been extracted from a DFT/BP86 calculation. Even though all calculations have been performed for the staggered D_{5h} conformation of ferrocene, we will follow the common convention of using the symmetry labels referring to the eclipsed D_{5d} conformation.⁸¹ For ferrocene, the pre-edge peak corresponds to a transition from the Fe 1s core orbital to the lowest unoccupied molecular orbital (LUMO). This LUMO is the degenerate e_{1g} -orbital, and is the

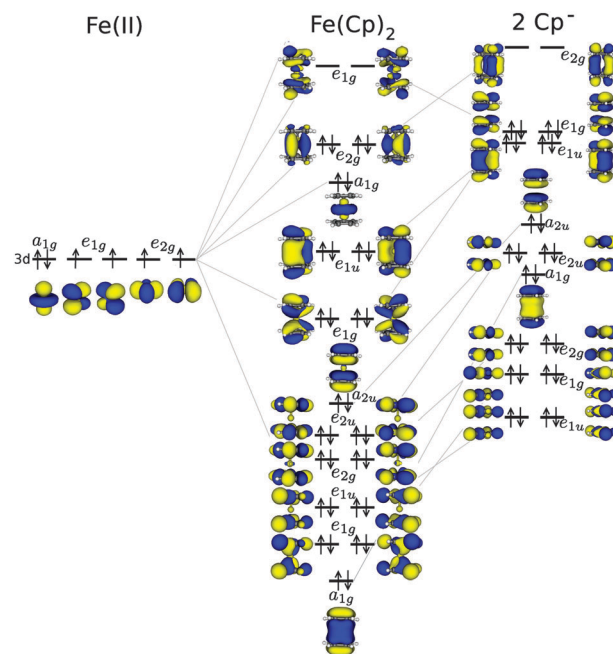


Fig. 5 Molecular orbital (MO) diagram of ferrocene focusing on the occupied valence orbitals. The ordering of the orbitals as well as the isosurface plots of the MOs have been obtained from a DFT calculation using the BP86 exchange–correlation functional.

anti-bonding combination of the iron d_{yz} and d_{xz} orbitals with cyclopentadienyl π orbitals. Such a $1s \rightarrow 3d$ transition is dipole forbidden, but has quadrupole intensity.^{20,43,77} The differences observed in the HERFD-XANES spectra of the other complexes arise from perturbations of this e_{1g} orbital due to the presence of the substituent group. In acetyl- and vinylferrocene, the anti-bonding π^* -orbital of the substituents interacts with one of the degenerate e_{1g} orbitals and splits it into two orbitals appearing at different energies. Consequently, two distinct peaks are

observed in the pre-edge region. This assignment of the HERD-XANES pre-edge peaks is shown in the upper part of Fig. 6 for ferrocene and vinylferrocene. Note that in the TD-DFT calculations, the splitting between the two pre-edge peaks depends sensitively on the choice of the functional. While BP86 underestimates this splitting with 0.84 eV, B3LYP overestimates it with 3.61 eV, compared to an experimental splitting of 1.8 eV.

With these results in mind, it can be expected that such substituents on the cyclopentadienyl rings will lead to significant perturbations to the occupied MOs as well. First, we consider the occupied molecular orbitals of ferrocene, shown in Fig. 5 (see also the discussion in ref. 40). The highest occupied molecular orbital (HOMO), e_{2g} , and the HOMO - 1, a_{1g} , are combinations of the remaining iron d-orbitals, namely of the $d_{x^2-y^2}$ and d_{xy} orbitals, and of the d_{z^2} orbital, respectively, with the cyclopentadienyl π -orbitals. The MOs at lower energies are composed primarily of the cyclopentadienyl π -orbitals

followed by cyclopentadienyl σ -orbitals at even lower orbital energies. For the occupied orbitals with e_{1u} or a_{2u} symmetry (*i.e.*, those with the same symmetry as the Fe p-orbitals and the electric-dipole operator) there are also small contributions from the iron p-orbitals.⁴⁰ The occupied e_{1g} orbital is the only one of the occupied orbitals within the relevant energy range shown here that has large d-orbital contributions. In fact, this e_{1g} orbital is the bonding combination of the iron d_{xz} and d_{yz} orbitals with cyclopentadienyl π -orbitals, whereas the unoccupied e_{1g} orbitals discussed above is the corresponding anti-bonding combination.

The background-corrected experimental (left) and calculated V2C-XES spectra (right) of ferrocene (a) and the substituted ferrocenes (b)–(e) are compared in Fig. 7a. For the experimental spectra, the deconvolution of the spectra is included in the figure. There are five peaks in the deconvolution of the experimental spectra, with those at higher energies (*i.e.*, between *ca.* 7105 and 7108 eV) having the largest intensities.

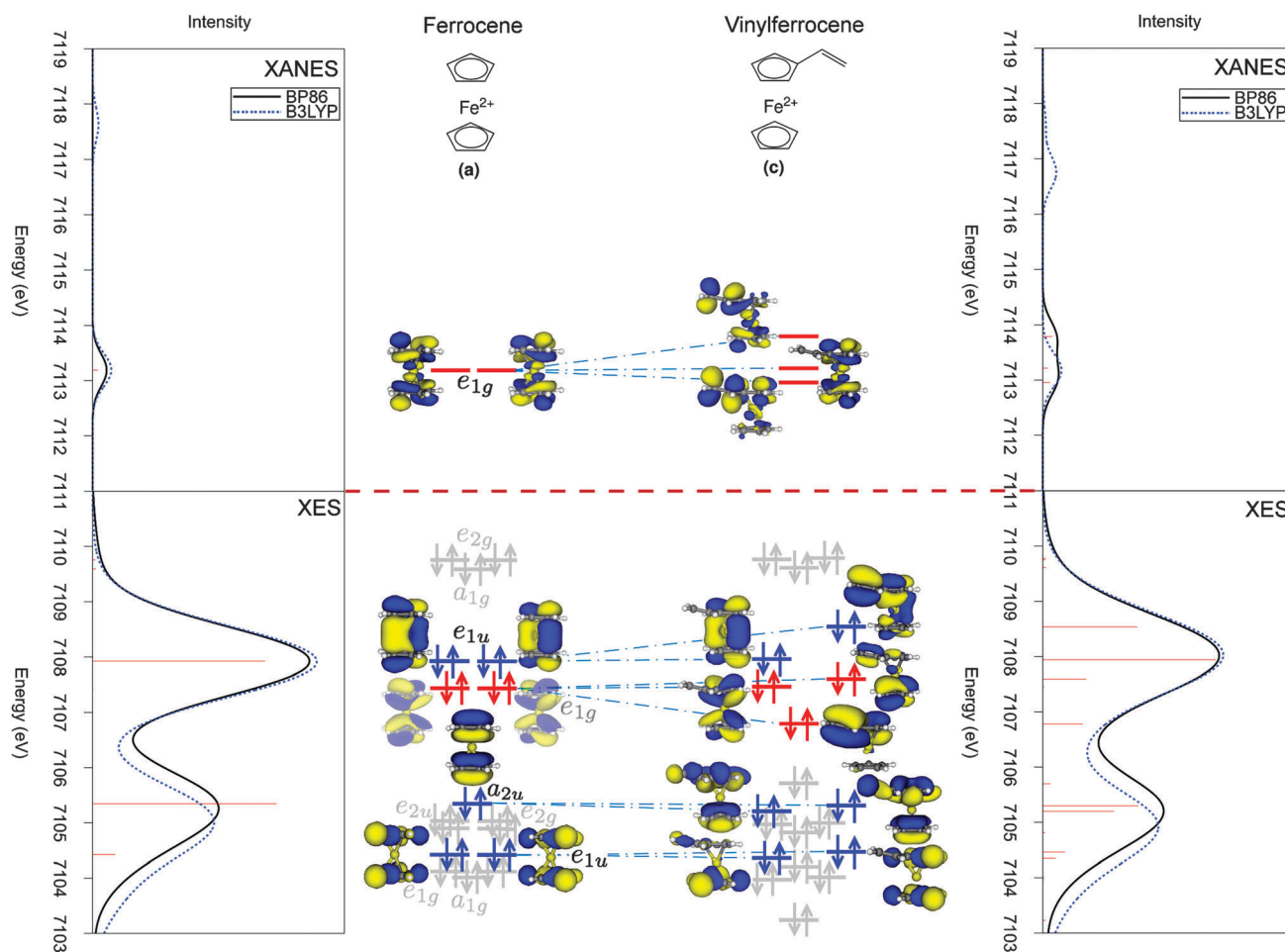


Fig. 6 Calculated pre-edge HERFD-XANES (top) and V2C-XES (bottom) spectra for ferrocene (left) and vinylferrocene (right). The calculated spectra are shown for both BP86 (black solid line) and for B3LYP (blue dashed line). For the BP86 calculation, the individual transitions are included as red sticks. Alongside the calculated spectra, the corresponding MO diagrams, as obtained from a DFT calculation with the BP86 exchange-correlation functional, are shown. In the MO diagram of ferrocene, the orbitals belonging to the same irreducible representations as the dipole operators (e_{1u} and a_{2u}) are highlighted in blue, whereas the e_{1g} orbitals are highlighted in red. All other orbitals do not contribute significantly to the spectra and are shown in grey. The same colors are used for the corresponding orbitals in vinylferrocene.

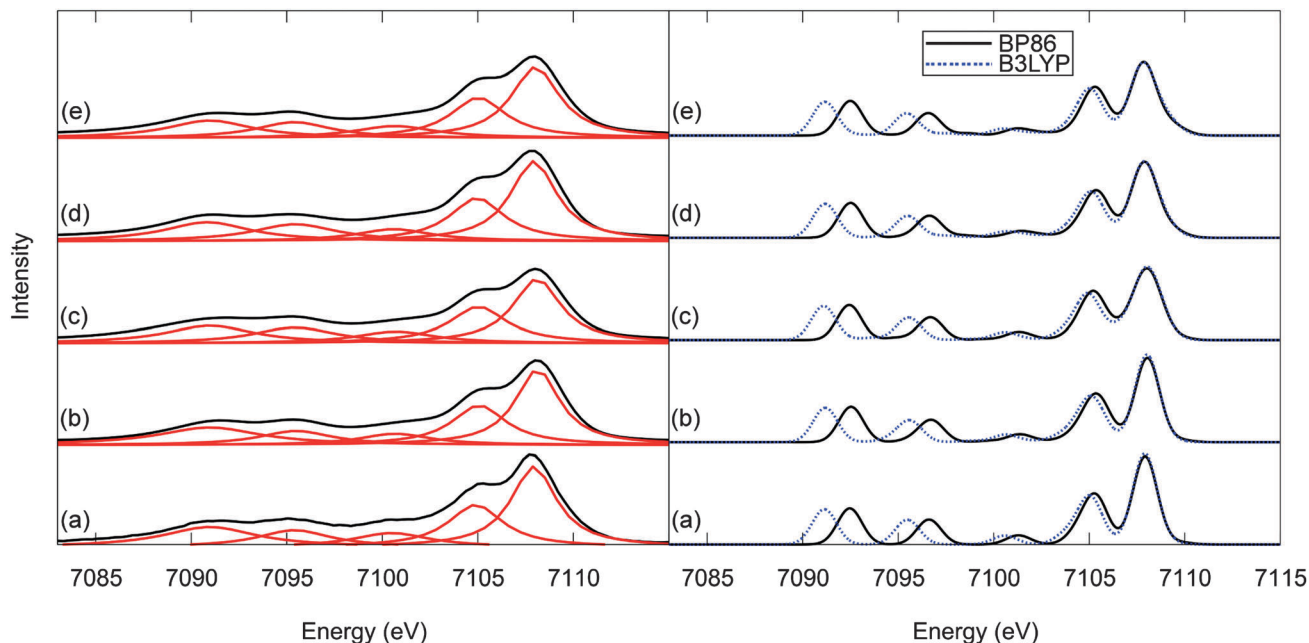


Fig. 7 Experimental (left) and calculated (right) V2C-XES spectra for the (substituted) ferrocenes (a)–(e). For the experimental spectra, the tail of the K β main line has been subtracted, and the deconvolution of the experimental spectrum is also included. The V2C-XES spectra calculated with DFT are shown both for the BP86 (black solid lines) and the B3LYP (blue dashed lines) exchange–correlation functionals.

The positions, intensities, and widths of the peaks as extracted from this deconvolution are listed in Table 1. We note that for ferrocene our results are consistent with those of ref. 40, with some deviations for the peaks at lower energies, which can be attributed to the different procedures used for subtracting the tail of the K β main line. The two intense peaks at higher energy can be fitted with a FWHM of about 3 eV, while the peaks at lower energies are significantly broader and show a FWHM of up to 6 eV.

Comparing the experimental spectra in Fig. 7, there is no observable difference between the experimental spectra of ferrocene and the differently substituted ferrocenes. This is confirmed when inspecting the positions and intensities extracted from the deconvolution given in Table 1. For the two peaks at *ca.* 7105 and 7108 eV the differences in the peak position are in all cases below 0.2 eV, which is within the experimental uncertainty. Slightly larger shifts occur for the lower energy peaks in some cases, especially for the third peak. However, this peak is rather weak and the shifts might be artifacts of the deconvolution. The intensities are very similar for all (substituted) ferrocenes as well. For the substituted ferrocenes the intensity of the highest-energy peak is decreased by up to *ca.* 15%, while the intensity differences are even smaller for all other peaks. Finally, difference spectra comparing the substituted ferrocenes (b)–(e) to ferrocene are shown in Fig. 3 in the ESI.† In all cases, these difference spectra only show a negative feature at *ca.* 7108 eV, corresponding to the decrease of the intensity of this peak. However, the difference spectra show no indication for shifts of peaks or for a significant broadening of individual peaks.

The calculated V2C-XES spectra are included in Fig. 7 and show a good agreement with experiment. In particular, the

intensity patterns are reproduced satisfactorily. This holds both for the calculations with the BP86 and with the B3LYP exchange–correlation functional. The only difference between the two functionals is a shift of the lower energy peaks. Comparing the calculated energies and intensities to those extracted by deconvoluting the experimental spectra (see Table 1), this good agreement between theory and experiment is confirmed. For the positions of the peaks at lower energies, B3LYP provides a better agreement with errors below 0.3 eV, whereas BP86 overestimates the energies of these peaks by up to 1.5 eV. Nevertheless, both functionals agree for the relative intensities of all peaks, and for both functionals the calculated intensities match those extracted from the experimental spectra with errors below 10–15%. The only exceptions are the intensities of the third peak at *ca.* 7101 eV, which are calculated significantly smaller than those extracted from the deconvolution of the spectra. This good agreement of the experimental and calculated spectra shows that, even though a rather large absolute shift had to be applied to the calculated spectra, the rather simple computational methodology applied here (see Section 2.2) is adequate for an assignment of the V2C-XES spectra.

To answer the question why the changes in the electronic structure due to substitution at the cyclopentadienyl ring are observable in HERFD-XANES but not in V2C-XES, we have to assign the V2C-XES spectra and relate the observed transitions to the underlying electronic structure. As a starting point, we consider the calculated spectrum of ferrocene, shown in Fig. 6 alongside the corresponding MO diagram. The two peaks at *ca.* 7108 eV and at *ca.* 7105 eV can be assigned to transitions from the occupied e_{1u} and a_{2u} orbitals, respectively, to the

Table 1 Energies (E_{rel} , in eV), intensities (Rel. int.), and full width at half maximum (FWHM, in eV) extracted from the deconvolution of the experimental spectra compared to the energies and intensities predicted with DFT calculations using the BP86 and B3LYP exchange–correlation functionals. All energies are given as shifts relative to the highest energy peak in ferrocene at 7107.94 eV, and intensities are normalized to the one of this peak

Complex	Experimental			DFT/BP86		DFT/B3LYP	
	E_{rel}	Rel. int.	FWHM	E_{rel}	Rel. int.	E_{rel}	Rel. int.
(a) Fe(Cp) ₂	0.00	1.00	2.87	0.00	1.00	0.00	1.00
	-3.05	0.63	3.45	-2.66	0.65	-2.91	0.63
	-7.44	0.29	4.83	-6.63	0.10	-7.34	0.10
	-12.54	0.34	4.60	-11.31	0.28	-12.44	0.27
	-16.96	0.51	5.90	-15.46	0.40	-16.78	0.38
(b) Fe(Cp)(CpAc)	0.20	0.91	2.78	0.12	0.96	0.11	0.97
	-2.86	0.58	3.42	-2.57	0.66	-2.84	0.64
	-7.25	0.22	4.56	-6.55	0.10	-7.29	0.09
	-12.42	0.28	4.52	-11.21	0.27	-12.35	0.26
	-16.91	0.44	5.91	-15.39	0.39	-16.73	0.37
(c) Fe(Cp)(CpVinyl)	0.17	0.84	3.02	0.10	1.02	0.11	1.02
	-2.99	0.57	3.62	-2.71	0.62	-3.00	0.59
	-7.22	0.25	5.01	-6.59	0.10	-7.31	0.09
	-12.51	0.35	5.19	-11.24	0.26	-12.37	0.25
	-16.95	0.42	5.55	-15.48	0.39	-16.82	0.37
(d) Fe(CpPPh ₂) ₂	-0.01	1.03	2.96	-0.03	0.98	-0.03	0.98
	-2.88	0.55	3.11	-2.56	0.63	-2.83	0.61
	-6.48	0.30	5.76	-6.46	0.10	-7.19	0.10
	-12.76	0.41	5.70	-11.29	0.26	-12.43	0.25
	-17.35	0.46	6.01	-15.41	0.39	-16.74	0.37
(e) Fe(CpP ⁱ Pr ₂) ₂	0.09	0.94	3.08	-0.07	0.99	-0.08	0.99
	-2.90	0.61	3.48	-2.62	0.61	-2.90	0.59
	-7.27	0.27	5.14	-6.63	0.11	-7.37	0.11
	-12.55	0.33	4.74	-11.35	0.25	-12.48	0.24
	-16.96	0.40	5.31	-15.43	0.38	-16.75	0.36

Fe 1s core orbital. These occupied e_{1u} and a_{2u} orbitals have the same symmetry as the dipole operator (*i.e.*, they belong to the same irreducible representation) and the corresponding transitions are, therefore, dipole-allowed. They gain intensity through the admixture of Fe p orbitals to the occupied e_{1u} and a_{2u} orbitals. For the second occupied e_{1u} -orbital, corresponding to a transition at 7104.4 eV, the Fe p-orbital contribution is negligible and the corresponding intensity almost vanishes. The occupied e_{1u} and a_{2u} orbitals, which correspond to these dipole-allowed transitions, are highlighted in blue in Fig. 6.

As discussed above, the occupied e_{1g} orbital is the only orbital in the considered energy range that has significant d orbital contributions. However, the transition from the occupied e_{1g} orbital to the 1s core orbital is dipole-forbidden and thus only has quadrupole intensity. Consequently, it is orders of magnitude weaker than the dipole-allowed transitions from the occupied e_{1u} and a_{2u} orbitals. Nevertheless, by analogy with the corresponding unoccupied e_{1g} orbital probed in the HERFD-XANES spectra, the occupied e_{1g} orbital might also be sensitive to substitutions at the cyclopentadienyl ligands. Therefore, it is highlighted in red in Fig. 6. For all other occupied orbitals in this energy range the transitions to the Fe 1s core orbital are dipole forbidden and their intensities are negligible.

These orbitals are shown in gray in Fig. 6. Note that the two peaks at lower energies (*i.e.*, at *ca.* 7092.5 eV and at *ca.* 7096.5 eV) are due to transitions from cyclopentadienyl σ -orbitals and are not included in Fig. 6.

For the ferrocene derivatives featuring π -substituents at the cyclopentadienyl ring (*i.e.* acetyl- and vinylferrocene), we expect significant changes to the occupied MOs. First, we consider vinylferrocene (c), for which the HERFD-XANES (top) and V2C-XES (bottom) spectra included shown in Fig. 6, alongside the corresponding MO diagram. In this MO diagram, we indicate the connection to the corresponding orbitals in ferrocene and use the same colors introduced above (*i.e.*, orbitals corresponding to dipole-allowed transitions in ferrocene are shown in blue, whereas orbitals corresponding to quadrupole transitions in ferrocene are shown in red). The substitution at the cyclopentadienyl ring makes a large impact on all of the occupied orbitals and compared to ferrocene, all relevant orbitals are perturbed. First, the degeneracy of the e_{1u} orbitals is lost due to mixing with the substituent π orbitals, and it is split into two orbitals separated by *ca.* 0.6 eV. Therefore, there are now two distinct transitions contributing to the highest energy peak in the V2C-XES spectrum, resulting in a slight broadening of the calculated peak. Second, the occupied a_{2u} orbital interacts with orbitals of the substituent and is split into two orbitals. However, the splitting is significantly smaller in this case, but none of these changes are observable in the spectrum because the occurring splitting of less than 1 eV is smaller than the resolution of the spectra.

In the HERFD-XANES spectra, the sensitivity to the π substituents is due to their effect on the unoccupied e_{1g} orbital. For the V2C-XES spectra, a similar splitting of the corresponding occupied e_{1g} orbital is found in the calculations. Indeed, the occupied e_{1g} orbital splits into two occupied orbitals in vinylferrocene and the resulting e_{1g} -like orbitals both have significant dipole intensity. These become observable as a contribution to the calculated spectra, but their intensity is still four times smaller than the one of the unperturbed e_{1u} -like orbital. Therefore, the e_{1u} peak dominates in this region and hides this splitting of the occupied e_{1g} orbital. The only change to the calculated spectrum is a slight broadening of the peak, which cannot be resolved in experiment.

Finally, we note that while for the calculation of the HERFD-XANES spectra we found that the splitting between the two unoccupied e_{1g} -like orbitals is extremely dependent on the choice of the functional,²⁰ this is not the case of the corresponding occupied orbitals. Here, the splitting between the occupied e_{1g} -like orbitals calculated with BP86 and with B3LYP only differ by approximately 0.1 eV.

For acetylferrocene (b), the second example of a ferrocene bearing a π substituent at the cyclopentadienyl ring, a similar picture is obtained. The assignment of the calculated spectra to MOs is shown in Fig. 10 in the ESI.† Here, the occupied orbitals introduced by the π substituent appear at a lower energy and interact with the occupied a_{2u} orbital. This leads to a splitting of *ca.* 0.7 eV for the transition corresponding to the second peak (*i.e.*, the one at *ca.* 7105 eV) in the V2C-XES spectrum, resulting

in a slight broadening of this peak. However, as for vinylferrocene, this broadening is not resolved in the experimental spectrum. The occupied e_{1u} orbitals are only slightly affected (with a splitting smaller than 0.1 eV) and the quadrupole transition from the occupied e_{1g} orbital to the 1s core orbital does not gain dipole intensity by mixing with substituent π orbitals.

For $\text{Fe}(\text{CpPPH}_2)_2$ and $\text{Fe}(\text{CpP}^i\text{Pr}_2)_2$, in which phosphine substituents have been introduced at the cyclopentadienyl rings, the pre-edge peaks in HERFD-XANES spectra are unchanged²⁰ (*i.e.*, the substituent orbitals do not alter the unoccupied e_{1g} orbital significantly). The same observation can be made for the occupied orbitals probed in the V2C-XES spectra. For $\text{Fe}(\text{CpP}^i\text{Pr}_2)_2$, the assignment of the calculated spectra is shown in Fig. 11 in the ESI.† Here, the occupied orbitals corresponding to intense transitions in the V2C-XES spectra appear at almost the same energies as in ferrocene. However, there are many additional occupied orbitals originating from the substituents. Some of these gain a small intensity by mixing with occupied orbitals with contributions at the iron atom, but these are small compared to the intense transitions from the occupied e_{1u} - and a_{2u} -like orbitals. For $\text{Fe}(\text{CpPPH}_2)_2$, there is an even larger number of occupied orbitals within the relevant energy range, but the overall picture is very similar and none of the additional occupied orbitals affects the V2C-XES spectra.

In summary, while for the examples considered here the substituents at the cyclopentadienyl ring(s) do affect the occupied orbitals, these differences cannot be resolved in the experimental V2C-XES spectra. In some cases, occupied orbitals that are degenerate in ferrocene are split, but the splitting is smaller than 0.6 eV. In other cases, in particular for the occupied e_{1g} orbital in vinylferrocene (corresponding to a quadrupole transition in ferrocene), the splitting is larger, but is hidden by more intense dipole-allowed transitions at a similar energy.

To estimate the experimental resolution required to detect these differences, the calculated spectra plotted using different broadenings for the individual transitions are shown in Fig. 4–9 in the ESI† together with the corresponding difference spectra. With a FWHM of 3.0 eV, corresponding to the experimental spectra reported here, only a very small broadening of the most intense peak can be observed in the difference spectra. This becomes more pronounced when decreasing the FWHM, but only for a FWHM of 1.0 eV indications for the splitting of some transitions appear in the difference spectra. Finally, for a FWHM of 0.5 eV these additional transitions can be identified as separate peaks in the calculated spectra.

4 Conclusions

In order to investigate the chemical sensitivity of V2C-XES and HERFD-XANES to substitutions beyond the first coordination shell we have considered ferrocene and four ferrocene derivatives in which substituents have been introduced at the cyclopentadienyl rings. While for HERFD-XANES, we have previously shown that the pre-edge peaks are sensitive to such changes, this is not the case for V2C-XES. In the former case, substituents at the cyclopentadienyl ring containing π -bonds lead to a

splitting of one of the e_{1g} orbitals, but such changes are not observable in the V2C-XES spectra. In contrast, there are no visible changes in the experimental spectrum due to the change in the second coordination shell.

To understand this different chemical sensitivity, the experiments have been complemented with DFT calculations, which allow for an assignment of the transitions to molecular orbitals. For the calculation of V2C-XES spectra, the simple Δ DFT approach of ref. 36 already provides a good agreement with experiment. In contrast to the calculation of HERFD-XANES, these calculations are less sensitive to the choice of the exchange–correlation functional and the calculations are in quantitative agreement with experiment.

The pre-edge peaks in HERFD-XANES probe dipole-forbidden transitions to unoccupied d-orbitals. In particular, for the LUMO in ferrocene, one of the degenerate e_{1g} orbital splits into two e_{1g} -like orbitals in acetyl- and vinylferrocene because of mixing with the substituent's π -orbitals. On the other hand, the V2C-XES spectra are dominated by dipole-allowed transitions originating from occupied ligand orbitals, with small Fe p-orbital contributions. These orbitals are less affected by substituents beyond the first coordination shell. Even though a splitting of the occupied e_{1g} orbital occurs due to substitution with an acetyl or vinyl group, it is not observable in the V2C-XES spectra. The increased intensity of the split e_{1g} -like orbitals are still significantly smaller than the dipole allowed transition corresponding to the unperturbed e_{1u} -like orbital.

For resolving the differences in the occupied orbitals caused by substitutions beyond the first coordination shell, it would be necessary to increase the resolution of experimental V2C-XES spectra. In principle, this would be possible by using analyzer crystals with a higher intrinsic resolution due to applied Bragg reflection, but at the price of reduced flux. However, even in this case, the lifetime broadening of the 1s core hole would still limit the experimental resolution. Since in HERFD-XANES the lifetime broadening of the 1s core hole is removed to a large extent, the resolution of V2C-XES would always be less than in HERFD-XANES.

While the specific results discussed here apply only to the considered example of substituted ferrocenes, we expect some observations to be more general. First, the pre-edge region in K-edge XAS spectra of transition metal complexes contains in most cases only the dipole-forbidden transitions to metal d orbitals. These will in general be very sensitive to substitution, both for directly coordinated ligands and possibly also beyond the first coordination shell. Therefore, with the possibility to resolve such subtle changes in these orbitals with HERFD-XANES measurements provides a very sensitive analytical tool. On the other hand, the V2C-XES spectra are dominated by dipole-allowed transitions originating from orbitals with contributions from metal p orbitals. Thus, changes in occupied metal d orbitals will hardly be detectable because the corresponding transitions are much weaker. We note that a smaller sensitivity of XES compared to XAS to structural changes has also been observed for the nitrogen K-edge of alanine peptides in solution.⁸²

To conclude, we have shown that, in contrast to HERFD-XANES, the V2C region of XES cannot distinguish changes in the electronic structure due to substitution in the second coordination shell, at least for the substituted ferrocenes considered here. Thus, the sensitivity of the pre-edge in HERFD-XANES provides unique opportunities for studying the electronic structure of transition metal complexes and for overcoming the current limitations of XAS. Even though V2C-XES is less sensitive to changes in the second coordination shell, it provides information on the occupied electronic states. In this respect it is, therefore, complementary to HERFD-XANES. Moreover, V2C-XES can still be a useful tool for distinguishing different oxidation states of transition metal centers, as shown here for ferrocene and ferrocenium, and for determining the identity and geometrical arrangement of the ligands in the first coordination shell.

Acknowledgements

The ESRF (Grenoble) is acknowledged for provision of beamtime in the frame of project CH-3219 (09-2010), and we thank Dr Kristina Kvashnina and Dr Pieter Glatzel for help and support during the measurements. AJA and CRJ thank the DFG-Center for Functional Nanostructures for funding. MB acknowledges funding from the Carl-Zeiss foundation in the frame of the junior professorship "Analytics of catalytic active materials".

References

- J.-D. Grunwaldt, D. Lützenkirchen-Hecht, M. Richwin, S. Grundmann, B. S. Clausen and R. Frahm, *J. Phys. Chem. B*, 2001, **105**, 5161–5168.
- X-ray Absorption: Principles, Applications, Techniques of EXAFS, SEXAFS, and XANES*, ed. D. C. Koningsberger and R. Prins, John Wiley & Sons Inc., New York, 1988.
- J. Singh, C. Lamberti and J. A. van Bokhoven, *Chem. Soc. Rev.*, 2010, **39**, 4754–4766.
- M. Bauer and C. Gastl, *Phys. Chem. Chem. Phys.*, 2010, **12**, 5575–5584.
- M. W. Tew, M. Janousch, T. Huthwelker and J. A. van Bokhoven, *J. Catal.*, 2011, **283**, 45–54.
- B. P. C. Hereijgers, T. M. Eggenhuisen, K. P. de Jong, H. Talsma, A. M. J. van der Eerden, A. M. Beale and B. M. Weckhuysen, *J. Phys. Chem. C*, 2011, **115**, 15545–15554.
- M. Bauer, R. Schoch, L. Shao, B. Zhang, A. Knop-Gericke, M. Willinger, R. Schlögl and D. Teschner, *J. Phys. Chem. C*, 2012, **116**, 22375–22385.
- E. Kleyenov, J. Sa, J. Abu-Dahrieh, D. Rooney, J. A. van Bokhoven, E. Troussard, J. Szlachetko, O. V. Safonova and M. Nachtegaal, *Catal. Sci. Technol.*, 2012, **2**, 373–378.
- J. O. Moulin, J. Evans, D. S. McGuinness, G. Reid, A. J. Rucklidge, R. P. Tooze and M. Tromp, *Dalton Trans.*, 2008, 1177–1185.
- S. H. Eitel, M. Bauer, D. Schweinfurth, N. Deibel, B. Sarkar, H. Kelm, H.-J. Krüger, W. Frey and R. Peters, *J. Am. Chem. Soc.*, 2012, **134**, 4683–4693.
- H. Junge, N. Marquet, A. Kammer, S. Denurra, M. Bauer, S. Wohlrab, F. Gärtner, M.-M. Pohl, A. Spannenberg, S. Gladiali and M. Beller, *Chem.–Eur. J.*, 2012, **18**, 12749–12758.
- J. Szlachetko, M. Nachtegaal, J. Sá, J.-C. Dousse, J. Hozzowska, E. Kleyenov, M. Janousch, O. V. Safonova, C. König and J. A. van Bokhoven, *Chem. Commun.*, 2012, **48**, 10898–10900.
- A. Mijovilovich, H. Hayashi, N. Kawamura, H. Osawa, P. C. A. Bruijninx, R. J. M. Klein Gebbink, F. M. F. de Groot and B. M. Weckhuysen, *Eur. J. Inorg. Chem.*, 2012, 1589–1597.
- F. Di Benedetto, F. D'Acapito, G. Fornaciai, M. Innocenti, G. Montegrossi, L. A. Pardi, S. Tesi and M. Romanelli, *Phys. Chem. Miner.*, 2009, **37**, 283–289.
- M. Wilke, F. Farges, P.-E. Petit, G. E. Brown and F. Martin, *Am. Mineral.*, 2001, **86**, 714–730.
- G. Giuli, E. Paris, K. U. Hess, D. B. Dingwell, M. R. Cicconi, S. G. Eeckhout, K. T. Fehr and P. Valenti, *Am. Mineral.*, 2011, **96**, 631–636.
- R. Sarangi, L. Yang, S. G. Winikoff, L. Gagliardi, C. J. Cramer, W. B. Tolman and E. I. Solomon, *J. Am. Chem. Soc.*, 2011, **133**, 17180–17191.
- A. Dey, Y. Peng, W. E. Broderick, B. Hedman, K. O. Hodgson, J. B. Broderick and E. I. Solomon, *J. Am. Chem. Soc.*, 2011, **133**, 18656–18662.
- M. Bauer, S. Müller, G. Kickelbick and H. Bertagnolli, *New J. Chem.*, 2007, **31**, 1950–1959.
- A. J. Atkins, Ch. R. Jacob and M. Bauer, *Chem.–Eur. J.*, 2012, **18**, 7021–7025.
- M. Rohr, J.-D. Grunwaldt and A. Baiker, *J. Catal.*, 2005, **229**, 144–153.
- J.-D. Grunwaldt and A. Baiker, *Phys. Chem. Chem. Phys.*, 2005, **7**, 3526–3539.
- P. Glatzel and U. Bergmann, *Coord. Chem. Rev.*, 2005, **249**, 65–95.
- K. Hämäläinen, D. P. Siddons, J. B. Hastings and L. E. Berman, *Phys. Rev. Lett.*, 1991, **67**, 2850–2853.
- H. Hayashi, Y. Udagawa, W. A. Caliebe and C.-C. Kao, *Chem. Phys. Lett.*, 2003, **371**, 125–130.
- J. Singh, E. M. C. Alayon, M. Tromp, O. V. Safonova, P. Glatzel, M. Nachtegaal, R. Frahm and J. A. van Bokhoven, *Angew. Chem., Int. Ed.*, 2008, **47**, 9260–9264.
- J. Singh, M. Tromp, O. V. Safonova, P. Glatzel and J. A. van Bokhoven, *Catal. Today*, 2009, **145**, 300–306.
- R. Jenkins, R. Manne, R. Robin and C. Senemaud, *X-Ray Spectrom.*, 1991, **20**, 149–155.
- M. A. Beckwith, M. Roemelt, M.-N. Collomb, C. DuBoc, T.-C. Weng, U. Bergmann, P. Glatzel, F. Neese and S. DeBeer, *Inorg. Chem.*, 2011, **50**, 8397–8409.
- C. J. Pollock and S. DeBeer, *J. Am. Chem. Soc.*, 2011, **133**, 5594–5601.
- N. A. Besley and F. A. Asmuruf, *Phys. Chem. Chem. Phys.*, 2010, **12**, 12024.
- V. Carravetta, H. Ågren and V. Barone, *Computational Strategies for Spectroscopy: from Small Molecules to Nano Systems*, Wiley, Hoboken, New Jersey, 2011, pp. 137–205.

- 33 S. DeBeer George, T. Petrenko and F. Neese, *J. Phys. Chem. A*, 2008, **112**, 12936–12943.
- 34 S. DeBeer George, T. Petrenko and F. Neese, *Inorg. Chim. Acta*, 2008, **361**, 965–972.
- 35 S. DeBeer George and F. Neese, *Inorg. Chem.*, 2010, **49**, 1849–1853.
- 36 N. Lee, T. Petrenko, U. Bergmann, F. Neese and S. DeBeer, *J. Am. Chem. Soc.*, 2010, **132**, 9715–9727.
- 37 M. U. Delgado-Jaime, B. R. Dible, K. P. Chiang, W. W. Brennessel, U. Bergmann, P. L. Holland and S. DeBeer, *Inorg. Chem.*, 2011, **50**, 10709–10717.
- 38 M. Roemelt, M. A. Beckwith, C. Duboc, M.-N. Collomb, F. Neese and S. DeBeer, *Inorg. Chem.*, 2012, **51**, 680–687.
- 39 R. K. Hocking, S. D. George, Z. Gross, F. A. Walker, K. O. Hodgson, B. Hedman and E. I. Solomon, *Inorg. Chem.*, 2009, **48**, 1678–1688.
- 40 K. M. Lancaster, K. D. Finkelstein and S. DeBeer, *Inorg. Chem.*, 2011, **50**, 6767–6774.
- 41 K. M. Lancaster, M. Roemelt, P. Ettenhuber, Y. Hu, M. W. Ribbe, F. Neese, U. Bergmann and S. DeBeer, *Science*, 2011, **334**, 974–977.
- 42 R. C. J. Atkinson, V. C. Gibson and N. J. Long, *Chem. Soc. Rev.*, 2004, **33**, 313–328.
- 43 M. F. Ruiz-Lopez, M. Loos, J. Goulon, M. Benfatto and C. R. Natoli, *Chem. Phys.*, 1988, **121**, 419–437.
- 44 E. Otero, R. G. Wilks, T. Regier, R. I. R. Blyth, A. Moewes and S. G. Urquhart, *J. Phys. Chem. A*, 2008, **112**, 624–634.
- 45 E. Otero, N. Kosugi and S. G. Urquhart, *J. Chem. Phys.*, 2009, **131**, 114313.
- 46 J. Estephane, E. Groppo, A. Damin, J. G. Vitillo, D. Gianolio, C. Lamberti, S. Bordiga, C. Prestipino, S. Nikitenko, E. A. Quadrelli, M. Taoufik, J. M. Basset and A. Zecchina, *J. Phys. Chem. C*, 2009, **113**, 7305–7315.
- 47 J. Estephane, E. Groppo, J. G. Vitillo, A. Damin, D. Gianolio, C. Lamberti, S. Bordiga, E. A. Quadrelli, J. M. Basset, G. Kervern, L. Emsley, G. Pintacuda and A. Zecchina, *J. Phys. Chem. C*, 2010, **114**, 4451–4458.
- 48 C. Gauthier, V. A. Solé, R. Signorato, J. Goulon and E. Mogueilina, *J. Synchrotron Radiat.*, 1999, **6**, 164–166.
- 49 P. Carra, M. Fabrizio and B. T. Thole, *Phys. Rev. Lett.*, 1995, **74**, 3700–3703.
- 50 G. Vankó, T. Neisius, G. Molnár, F. Renz, S. Kárpáti, A. Shukla and F. M. F. de Groot, *J. Phys. Chem. B*, 2006, **110**, 11647–11653.
- 51 Theoretical Chemistry, Vrije Universiteit Amsterdam, ADF, *Amsterdam density functional program*, Program.
- 52 C. F. Guerra, J. G. Snijders, G. t. Velde and E. J. Baerends, *Theor. Chem. Acc.*, 1998, **99**, 391–403.
- 53 G. te Velde, F. M. Bickelhaupt, E. J. Baerends, C. Fonseca Guerra, S. J. A. van Gisbergen, J. G. Snijders and T. Ziegler, *J. Comput. Chem.*, 2001, **22**, 931–967.
- 54 A. D. Becke, *Phys. Rev. A*, 1988, **38**, 3098–3100.
- 55 J. P. Perdew, *Phys. Rev. B: Condens. Matter Mater. Phys.*, 1986, **33**, 8822–8824.
- 56 M. Stener, G. Fronzoni and M. de Simone, *Chem. Phys. Lett.*, 2003, **373**, 115–123.
- 57 K. Ray, S. DeBeer George, E. Solomon, K. Wiegardt and F. Neese, *Chem.–Eur. J.*, 2007, **13**, 2783–2797.
- 58 P. Banerjee, S. Sproules, T. Weyhermüller, S. DeBeer George and K. Wiegardt, *Inorg. Chem.*, 2009, **48**, 5829–5847.
- 59 P. Chandrasekaran, S. C. E. Stieber, T. J. Collins, L. Que, Jr., F. Neese and S. DeBeer, *Dalton Trans.*, 2011, **40**, 11070.
- 60 C. C. Scarborough, S. Sproules, T. Weyhermüller, S. DeBeer and K. Wiegardt, *Inorg. Chem.*, 2011, **50**, 12446–12462.
- 61 C. C. Scarborough, S. Sproules, C. J. Doonan, K. S. Hagen, T. Weyhermüller and K. Wiegardt, *Inorg. Chem.*, 2012, **51**, 6969–6982.
- 62 A. D. Becke, *J. Chem. Phys.*, 1993, **98**, 5648.
- 63 C. Lee, W. Yang and R. G. Parr, *Phys. Rev. B: Condens. Matter Mater. Phys.*, 1988, **37**, 785–789.
- 64 E. van Lenthe, E. J. Baerends and J. G. Snijders, *J. Chem. Phys.*, 1993, **99**, 4597–4610.
- 65 E. van Lenthe, E. J. Baerends and J. G. Snijders, *J. Chem. Phys.*, 1994, **101**, 9783–9792.
- 66 H. Ågren, V. Carravetta, O. Vahtras and L. G. Pettersson, *Chem. Phys. Lett.*, 1994, **222**, 75–81.
- 67 H. Ågren, V. Carravetta, O. Vahtras and L. G. M. Pettersson, *Theor. Chem. Acc.*, 1997, **97**, 14–40.
- 68 U. Ekström, P. Norman and V. Carravetta, *Phys. Rev. A*, 2006, **73**, 022501.
- 69 M. Stener, A. Lisini and P. Decleva, *Chem. Phys.*, 1995, **191**, 141–154.
- 70 L. Triguero and L. G. Pettersson, *Surf. Sci.*, 1998, **398**, 70–83.
- 71 M. Leetmaa, M. P. Ljungberg, A. Lyubartsev, A. Nilsson and L. G. M. Pettersson, *J. Electron Spectrosc. Relat. Phenom.*, 2010, **177**, 135–157.
- 72 P. S. Bagus, *Phys. Rev.*, 1965, **139**, A619–A634.
- 73 N. A. Besley, A. T. B. Gilbert and P. M. W. Gill, *J. Chem. Phys.*, 2009, **130**, 124308.
- 74 U. Ekström, P. Norman, V. Carravetta and H. Ågren, *Phys. Rev. Lett.*, 2006, **97**, 143001.
- 75 U. Ekström and P. Norman, *Phys. Rev. A*, 2006, **74**, 042722.
- 76 B. Brena, P. E. M. Siegbahn and H. Ågren, *J. Am. Chem. Soc.*, 2012, **134**, 17157–17167.
- 77 S. Bernadotte, A. J. Atkins and Ch. R. Jacob, *J. Chem. Phys.*, 2012, **137**, 204106.
- 78 L. Triguero, L. G. M. Pettersson and H. Ågren, *Phys. Rev. B: Condens. Matter Mater. Phys.*, 1998, **58**, 8097–8110.
- 79 A. Nilsson and L. G. M. Pettersson, *Surf. Sci. Rep.*, 2004, **55**, 49–167.
- 80 G. Smolentsev, A. V. Soldatov, J. Messinger, K. Merz, T. Weyhermüller, U. Bergmann, Y. Pushkar, J. Yano, V. K. Yachandra and P. Glatzel, *J. Am. Chem. Soc.*, 2009, **131**, 13161–13167.
- 81 F. A. Cotton and G. Wilkinson, *Advanced Inorganic Chemistry*, John Wiley & Sons Inc., 1980.
- 82 W. Hua, Y.-J. Ai, B. Gao, H. Li, H. Ågren and Y. Luo, *Phys. Chem. Chem. Phys.*, 2012, **14**, 9666–9675.